Progress In Electromagnetics Research, Vol. 132, 275–296, 2012

FREQUENCY SCANNING BASED RADAR SYSTEM

Y. Álvarez Lopez*, C. García, C. Vázquez, S. Ver-Hoeye, and F. Las-Heras

Área de Teoría de la Señal y Comunicaciones, Universidad de Oviedo, Edif, Polivalente, Mod. 8, Campus Universitario de Gijón, E-33203, Gijón, Asturias, Spain

Abstract—A novel imaging technique based on a frequency scanning antenna array is presented. The method is conceived to provide angular information in range-based radar systems which do not allow mechanical or electronic beam steering. The beam steering is changed with frequency, which requires a novel scattered field data processing scheme/algorithm to recover the SAR image. System features, advantages and limitations are discussed, presenting simulation and measurement results, which show the system capabilities to resolve the range and angular position of the objects.

1. INTRODUCTION

The use of microwaves and mm-waves in imaging systems has become very common nowadays due to the advantages of this frequency band as non-ionizing electromagnetic field, the use of mature technology and the capacity to penetrate dielectric bodies. Because of these reasons, electromagnetic inverse techniques are attractive for non-invasive applications in different fields, such as security and defense applications for detecting concealed weapons and buried objects [1, 2], and medical diagnostics [3].

This contribution focuses on the profile reconstruction of metallic objects, which can be of interest for the detection of concealed weapons and buried objects. There are several techniques to deal with the profile reconstruction problem of metallic objects: one is the Linear Sampling Method [4], which determines if a point on the investigation domain belongs to the object-under-test (OUT) or not by solving a linear system of equations.

Received 18 July 2012, Accepted 13 September 2012, Scheduled 1 October 2012

* Corresponding author: Yuri Álvarez Lopez (yurilope@gmail.com).

Other group of techniques is based on the so-called inverse source methods [5–9]. In this case, a set of equivalent electric currents is reconstructed in a domain containing the OUT from the scattered field samples. The highest amplitude values of the reconstructed currents correspond to the actual OUT profile.

Several techniques are based on an initial guess of the OUT profile defined in base of some parameters (e.g., Fourier coefficients, splines, etc.). Then, this set of parameters is modified until finding one that satisfies an imposed boundary condition [10, 11]. The main drawback of these methods is the need of solving a non-linear system of equations, usually carried out by means of global search techniques that minimize a cost function relating the boundary conditions and the profile parameters. The Contrast Source Inversion (CSI), a well-known profile reconstruction technique [12] can be classified in this category.

Finally, Synthetic Aperture Radar (SAR) is one of the most widely used radar imaging methods [13–15]. Again, a linear expression relating the scattered field acquisition domain and the reconstruction domain (where the SAR image is formed) is used, allowing the use of a Fast Fourier Transform in the case of canonical domains (planar, cylindrical, spherical), providing fast imaging capabilities. Due to the advantages of simplicity and fast calculations, this is the reconstruction method to be used in this contribution.

Apart from the methods used for processing the information, another classification of inverse techniques comes from the setup configuration. In general, accurate profile reconstruction requires range (depth) and cross-range (angular position) information. Under the assumption of mechanically fixed transmitter and receiver in a monostatic configuration, range information is provided by the radar system bandwidth. Cross-range information can be achieved: i) By using fixed-beam antennas, and placing the OUT on top of a rotary platform. ii) By means of beamscanning systems. Sometimes, rotation of the OUT is not possible, thus leaving beamscanning methods as the only way to gather cross-range information, which is given by the knowledge of the beam steering angle [16, 17].

This contribution analyzes the possibility of obtaining range and cross-range information using frequency scanning antenna arrays. Frequency scanning antennas have been widely used for different applications [18–21] but hardly for imaging purposes [22]. Here, the idea is to scan the OUT so that the beam steering angle changes with frequency, illuminating different regions of the OUT for different frequencies. In consequence, frequency scanning imaging systems exhibit a trade-off between available range and cross-range information, which is studied in this contribution.

2. DESCRIPTION OF THE METHOD

The method proposed in this contribution is based on the use of a frequency scanning antenna array (FSAA). In this configuration, the transmitting and receiving antennas are fixed, and no mechanical or phaseshifters-based electronically beam steering alteration of the acquisition set-up is allowed.

This type of configuration in which no beam scanning is involved leads to a range-based radar, providing information in terms of the distance from the targets to the radar, i.e., range information.

Angular position information is provided by beam steering-based systems. In the case of mechanically rotated antennas (e.g., primary radars), the main drawback is the cost of the radiofrequency rotary joint and the mechanical parts maintenance, especially at high

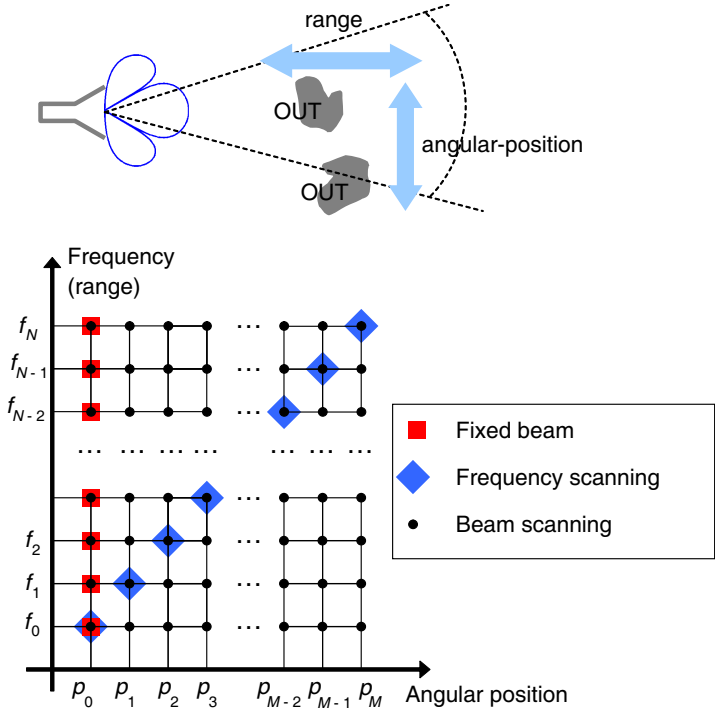

Figure 1. Analysis of the range and angular position information available depending on the measurement system to be used. Frequency scanning is an intermediate system in terms of amount of information provided.

frequencies. The use of active antenna arrays with electronically-controlled phase shifters is another option, but again the technological (and economical) complexity may limit its deployment [16, 17].

Figure 1 summarizes the concepts of range-based radars (fixed antenna beam) and beam-scanning systems, showing the amount of information provided in each case. It can be observed that beam-scanning systems are the extension of range-based radars for a set of angular positions (or steering directions). In the case of range-based radars, the system resolution is given by the frequency bandwidth. Angular resolution of beam scanning systems is determined by the antenna beamwidth.

Frequency scanning is an intermediate technique between beam scanning methods that provide good range and angular resolution and the use of an antenna with a constant beam direction, which only provides range resolution. The frequency scanning systems provide a trade-off between angular and range resolution, as shown in Figure 2.

The problem of the frequency scanning is intrinsic to the technique as the bandwidth for a fixed steering angle is zero (see Figure 1), or, in other words, changing the frequency modifies the beam steering.

To deal with this drawback, several solutions have been proposed. One is the traditional SAR processing [13–15]: the SAR image at every frequency is formed using the scattered field information. To combine the SAR images at every frequency, each one is multiplied by the conjugate of the incident field of the array (which also changes with frequency), then all the contributions are added [2, 23]. This technique has been tested, obtaining typically a blurred SAR image where the scatterers could not be clearly distinguished. In consequence, this kind

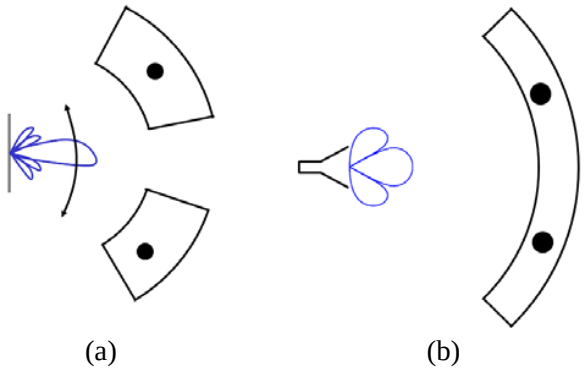

Figure 2. Resolution cells when using (a) frequency scanning antenna array, (b) horn antenna (or any other kind of fixed beam antenna).

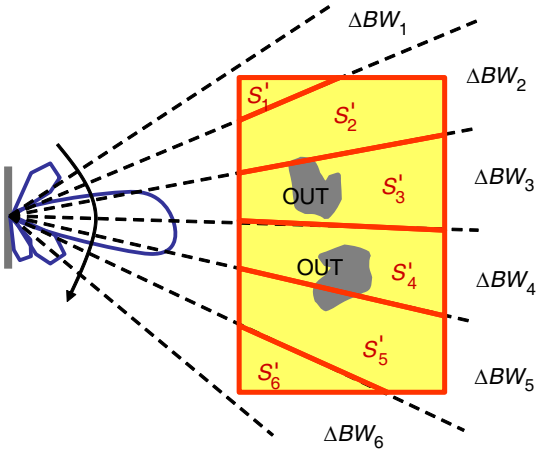

Figure 3. Subdivision of the frequency scanning bandwidth in frequency windows (ΔBW_n), each one having associated an angular region S'_n of the reconstruction domain.

of processing was discarded.

A second approach is based on a windowing technique. The method works under the assumption that, for a given frequency window ΔBW, the OUT region illuminated by the beam is assumed to be the same (it is considered that the beam position variation is small within ΔBW). In consequence, the whole frequency bandwidth of the FSAA is divided into several ΔBW_n windows, that are associated with angular regions (S'_n) defined on the reconstruction domain (see Figure 3).

The profile reconstruction for every n-th frequency window ΔBW_n is performed by using the traditional SAR imaging: a SAR image is retrieved in the entire reconstruction domain (not only in the current S'_n) using the scattered field information belonging to the ΔBW_n frequency window. If the angular region S'_n associated with the ΔBW_n frequency window is small enough, SAR image blurring due to the displacement of the beam steering inside the ΔBW_n frequency bandwidth is negligible in that S'_n domain.

Frequency scanning imaging requires the knowledge of the FSAA beam steering characteristics. An accurate way to determine its behavior is by measuring the antenna array radiation pattern in the frequency bandwidth, and calculating the beam steering angle for every frequency. Once the relationship between frequency and beam steering angle is known, it is possible to define the angular regions S'_n associated with every ΔBW_n.

The SAR image reflectivity on each angular region S'_n is then given by:

$$\rho^n_{rec}\left(\vec{r}'_q\right) = \left[\sum_{m=1}^{M} E_{meas}\left(f_m, \vec{r}\right) e^{j\left\langle E_{inc}\left(f_m, \vec{r}'_q\right)\right\rangle} e^{jk_0 R}\right] \cdot W\left(\vec{r}'_q\right)$$
$$f_m \in \Delta BW_n \quad W\left(\vec{r}'_q\right) = \begin{cases} 1 & \vec{r}'_q \in S'_n \\ 0 & \vec{r}'_q \notin S'_n \end{cases} \qquad R = \left|\vec{r} - \vec{r}'_q\right|, \tag{1}$$

where $E_{meas}\ (f_m, \vec{r})$ is the measured or simulated scattered field (copolar component) observed at the point defined by the position vector $\vec{r}$ at the frequency f_m. k_0 is the wavenumber, $k_0 = 2\pi/\lambda$. M is the number of discrete frequencies within the interval ΔBW_n. $\langle E_{inc}(f_m, \vec{r}'_q)\rangle$ is the phase of the incident electric field radiated by the FSAA, evaluated in the reconstruction domain point defined by the vector $\vec{r}'_q$. R is the distance between the position of the transmitting/receiving antennas ($\vec{r}$) and the reconstruction domain points ($\vec{r}'_q$). And $\rho^n_{rec}(\vec{r}'_q)$ is the reflectivity on the $\vec{r}'_q$ point associated with the ΔBW_n frequency window. A window function, $W(\vec{r}'_q)$,

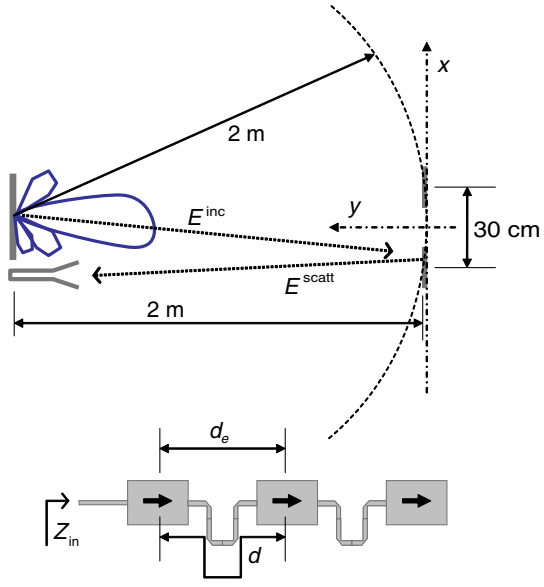

Figure 4. Upper plot: evaluation scheme of the frequency scanning antenna array (FSAA) imaging capabilities. Lower plot: basic layout of the FSAA.

is introduced to define the angular region S'_n associated with the corresponding frequency window ΔBW_n, so that the reflectivity values retrieved outside the current angular region are discarded.

Thus, the trade-off between range and cross-range accuracy depends on the frequency window bandwidth. Small ΔBW gives accurate angular position, but poor range resolution, and vice-versa.

3. RADAR SYSTEM EVALUATION

In order to analyze the frequency scanning imaging features, a theoretical frequency scanning array is used as transmitting antenna, assuming an omnidirectional antenna receiver. The array works in the 26 to 34 GHz frequency band. FSAA elements, emitting with TE polarization, are separated $d_e = 9\,\text{mm}$ ($d_e = 0.9\lambda$ at the center frequency of 30 GHz). The parameter d defines the series feed line length, that determines the FSAA phaseshift [24]. Figure 4 represents the proposed simulation test bed, in which detection capabilities of the FSAA are tested for different parameters: number of FSAA elements (N), series feed line length (d), and frequency window bandwidth (ΔBW).

The first step is the definition of the frequency — beam steering angle relationship. FSAA radiation pattern is evaluated from 26 to

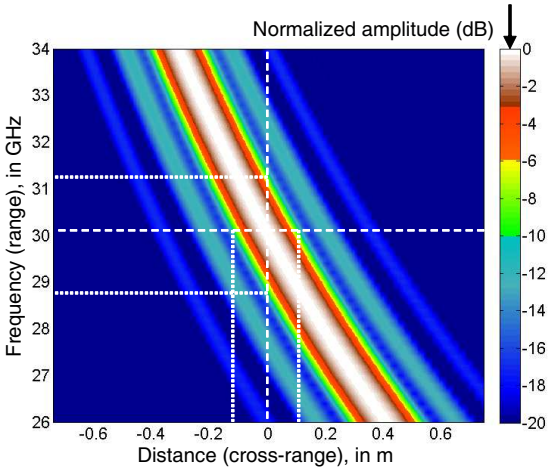

Figure 5. Normalized electric field (amplitude, in dB) radiated by the frequency scanning antenna array at different frequencies and distances along a line placed 2 m away from the Tx/Rx. $N = 15$, $d_e = 0.9\lambda$, $d = 1.2\lambda$.

34 GHz in 50 MHz steps. Figure 5 represents the frequency-distance relationship evaluated along a line placed 2 m away from the Tx/Rx antennas, which are placed in the position $x = 0$, $y = +2$ m (see Figure 4). Simulation FSAA parameters are $N = 15$, $d_e = 0.9\lambda$, $d = 1.2\lambda$. A phase correction is applied to have a broadside configuration at 30 GHz. The same analysis can be done for different FSAA parameters, obtaining different frequency-distance plots. Obviously, the FSAA beam steering is given by the maximum amplitude of the pattern (white color in Figure 5). From the results depicted in Figure 5, it is

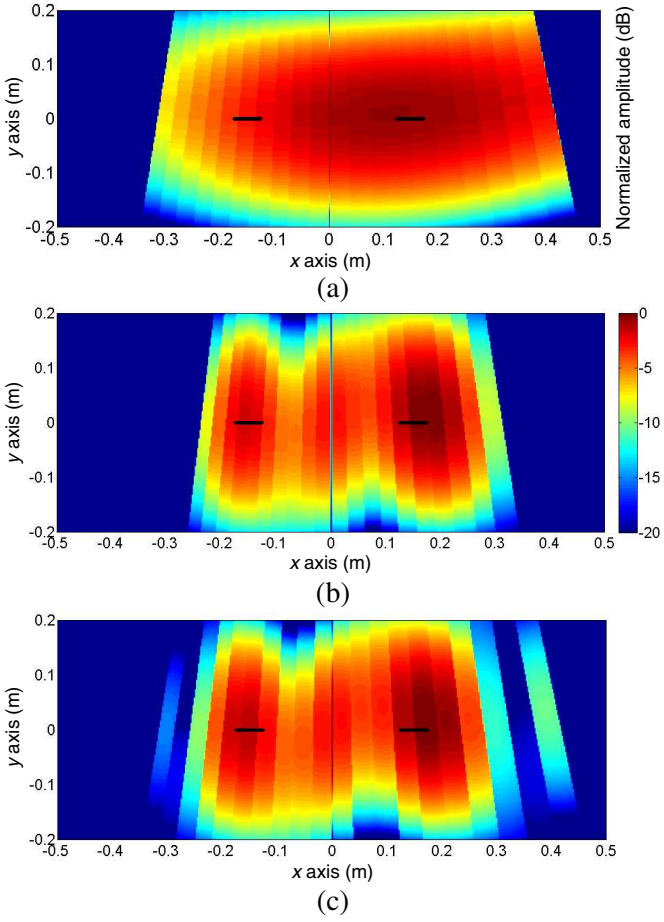

Figure 6. SAR image when the FSAA elements are (a) $N = 3$, (b) $N = 9$, (c) $N = 15$. For all the cases, $d_e = 0.9\lambda$, $d = 1.2\lambda$, $\Delta BW = 400$ MHz.

also possible to extract the cross-range resolution: assuming a −10 dB beamwidth criterion, the cross-range resolution is 20 cm at the center frequency (30 GHz), meaning that 2 objects separated more than 20 cm in cross-range could be distinguished.

The next step is the definition of the reconstruction domain. A 100×40 cm domain is defined, enclosing two metallic flat plates which are chosen to evaluate the FSAA imaging system detection capabilities. The metallic plates are 6 cm wide in x axis, and 20 cm long in the z axis (perpendicular to the reconstruction domain). Physical Optics code is used to synthesize the scattered field data (forward problem). A comparison with a commercial MoM has been performed, finding negligible discrepancies between the results provided by both methods.

First, imaging capabilities for different number of FSAA elements are tested. Figure 6 shows the reconstructed SAR images for $N = 3$, $N = 9$ and $N = 15$ elements, with $d_e = 0.9\lambda$, $d = 1.2\lambda$, $\Delta BW = 400$ MHz. In the first case (Figure 6(a)), the wide beamwidth of the FSAA antenna does not provide enough angular resolution to distinguish the two metallic bars, while FSAA with $N = 9$ and $N = 15$ do. It must be remarked that secondary lobes of the FSAA may produce echoes in the retrieved SAR image, as observed in Figure 6(c), so just increasing the number of FSAA elements does not ensure better resolution.

Next, the influence of the series feed line length (d) is analyzed. This parameter determines the frequency — beam steering angle

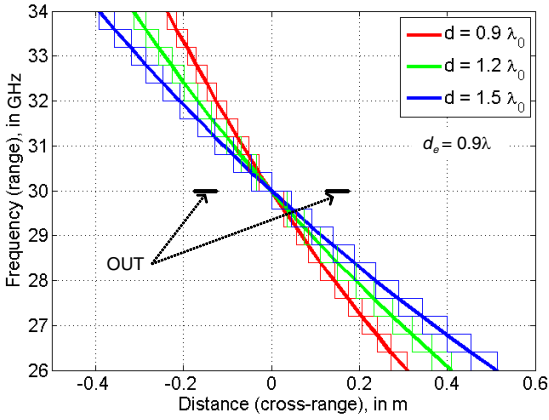

Figure 7. Analysis of the FSAA steering position as a function of d. $d_e = 0.9\lambda$, $\Delta BW = 400$ MHz, $N = 15$. Rectangles represent the frequency-distance interval for every $\Delta BW = 400$ MHz window.

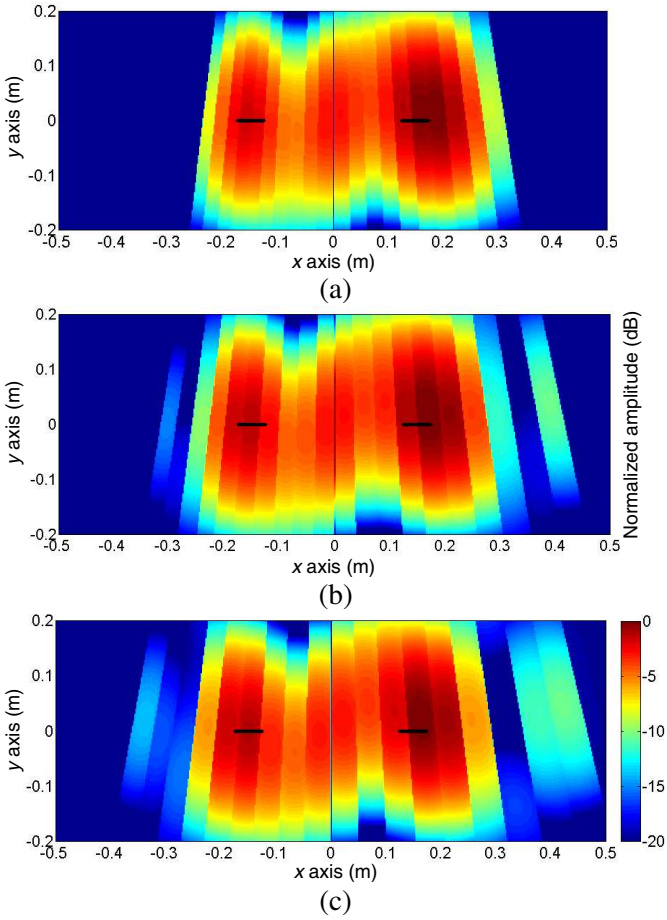

Figure 8. SAR image when the phaseshift is given by (a) $d = 0.9\lambda$, (b) $d = 1.2\lambda$, (c) $d = 1.5\lambda$. For all the cases, $N = 15$ elements, $d_e = 0.9\lambda$, $\Delta BW = 400\,\text{MHz}$.

relationship, as depicted in Figure 7. Longer feed line length increases the cross-range sweep margin, but also widens the S'_n regions for a given ΔBW_n.

Figure 8 represents the reconstructed SAR images for different d values. $N = 15$ elements FSAA is considered. It can be observed that the detection capabilities are not significantly distorted. The most significant effect is the variation in the S'_n regions width, so that the overall scanning region at $y = 0\,\text{m}$ goes from 45 cm (Figure 8(a), $d = 0.9\lambda$) to 85 cm (Figure 8(c), $d = 1.5\lambda$).

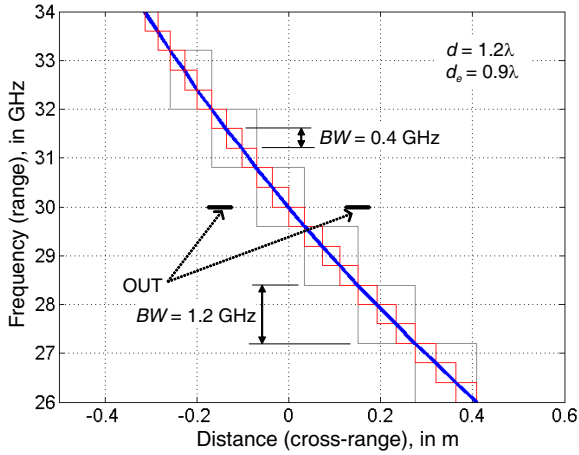

Figure 9. Analysis of the FSAA steering position as a function of the resolution window ($\Delta BW = 400\,\text{MHz}$ and $\Delta BW = 1.2\,\text{GHz}$). $d = 1.2\lambda$. $d_e = 0.9\lambda$, $N = 15$.

Finally, the influence of the frequency window bandwidth ΔBW is analyzed. For this purpose, $N = 15$, $d = 1.2\lambda$ parameters are chosen. Figure 9 represents the FSAA steering position vs. frequency together with the division in $\Delta BW = 400\,\text{MHz}$ and $\Delta BW = 1200\,\text{MHz}$, resulting in 20 and 6 angular regions respectively. SAR image results are depicted in Figure 10. In this case, the influence of the ΔBW in the range and cross-range resolution is clearly visible: a window of $\Delta BW = 400\,\text{MHz}$ provides reasonable x-axis distance resolution, allowing the identification of the two metallic bars. However, the position determination along y-axis (range) is not well-defined at all. If a wider ΔBW is chosen, range resolution is improved (see Figures 10(b) and (c)), but at the expense of loosing cross-range resolution. This fact can be observed in Figure 10(c), where the angular position of the two plates cannot be clearly distinguished. In addition, it must be remembered that increasing the ΔBW may yield a degradation of the retrieved SAR image, as the assumption of invariant beam illumination within ΔBW becomes not valid.

4. MEASUREMENT RESULTS

Once the FSAA for imaging purposes has been tested with simulations, a practical case based on measurements is presented. For this purpose,

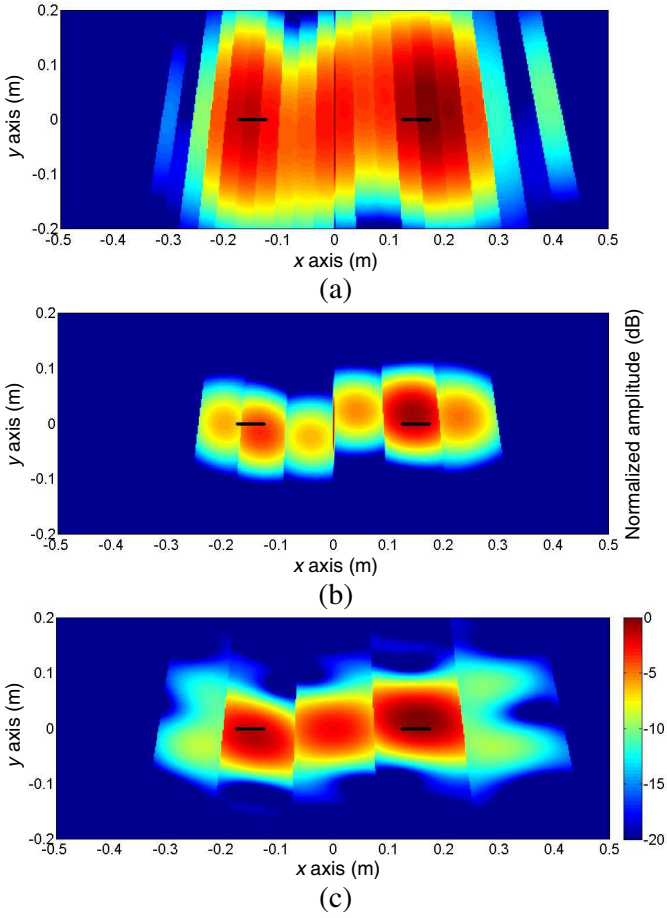

Figure 10. SAR image for different frequency window bandwidth: (a) $\Delta BW = 400\,\text{MHz}$, (b) $\Delta BW = 1200\,\text{MHz}$, (c) $\Delta BW = 1600\,\text{MHz}$. For all the case, $d = 1.2\lambda$. $d_e = 0.9\lambda$, $N = 15$.

an existing manufactured FSAA has been used [24].

The FSAA parameters are $N = 10$, $d_e = 11.6\,\text{mm}$, $d = 2\lambda_{g_0}$, where λ_{g_0} is the guided wavelength at the center frequency $f = 16.6\,\text{GHz}$ [24]. TE polarization is considered, being E_x the copolar component. The FSAA radiation pattern has been measured at the spherical range in anechoic chamber of the University of Oviedo, from 15 to 18 GHz, in 50 MHz steps. Figure 11 represents the steering angle as a function of the frequency.

From the results plotted in Figure 11 it is observed that the

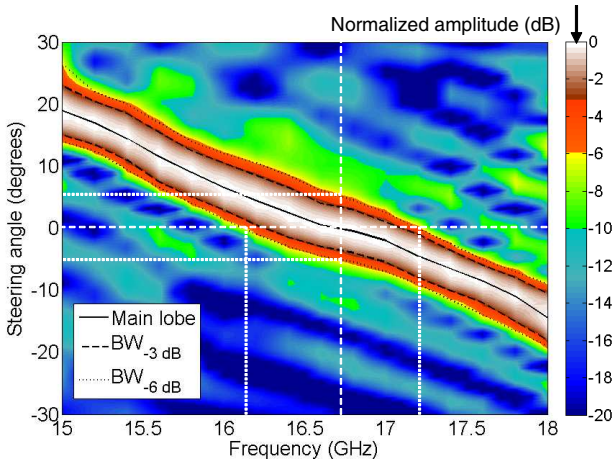

Figure 11. Normalized electric field in dB radiated by the FSAA at different frequencies and steering angles.

angular margin covered by the manufactured FSAA is 40 degrees. That means 70 cm cross-range at 1 m distance. The cross-range resolution can be extrapolated from the antenna -10 dB beamwidth, which is approximately 15 degrees (26 cm at 1 m). That means that the FSAA imaging system would be able to distinguish two objects separated more than 26 cm.

In order to provide a comparison, FSAA imaging capabilities are compared with the SAR image results provided by a radar system formed by two horn antennas. It is important to remark that, in all cases, the transmitter and receiver are fixed.

The FSAA and horn antenna used as transmitters are characterized by means of an equivalent magnetic currents distribution [25–27]. The E_x field component radiated on the XY plane is plotted in Figure 12 ($f = 18$ GHz).

As a first example, a metallic bar placed at $(x; y) = (0.3; 1.5)$ m with respect to the transmitting antenna is chosen. The bar is 2 m high in order to provide translation symmetry along z-axis, so that 2D approximation can be considered accurate enough. The measurement setup is shown in Figure 13.

The scattered field is always acquired using a horn as receiving antenna. The field is acquired in the 15 to 18 GHz frequency band, sampled each 50 MHz. Reconstruction results are depicted in Figure 15(a). In the case of using a horn antenna as transmitter, only range information is available (for representation purposes, the

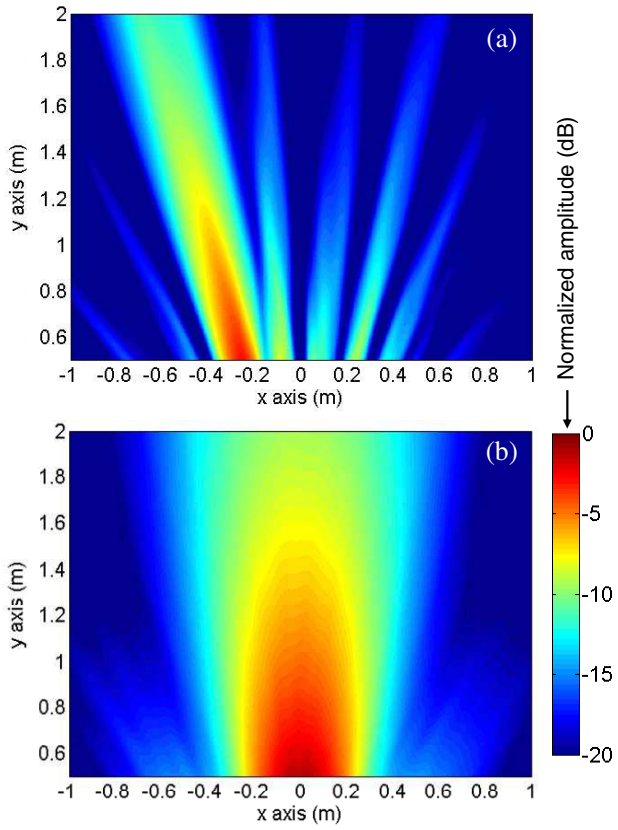

Figure 12. Electric field (E_x component, normalized amplitude in dB) radiated by (a) FSAA and (b) horn antenna. $f = 18\,\text{GHz}$.

2D SAR image is plotted as an arc, Figure 15(a)), that is, the bar is placed 1.5 m away from the transmitter, but no information about the angular position can be extracted.

Next step is the use of the FSAA antenna as transmitter. Figure 15(b) shows the SAR image when a frequency window of $\Delta BW = 300\,\text{MHz}$ is considered. Now, the SAR image not only provides range information, but also angular position, corresponding to the true placement of the metallic bar. Another echo is observed in the plot, on the right of the main spot. This is mainly due to the FSAA secondary lobes, which can be clearly appreciated in Figure 12.

Second, a more challenging example has been tested. Another metallic bar has been added, placed at $(x; y) = (-0.2; 1.5)\,\text{m}$, that is,

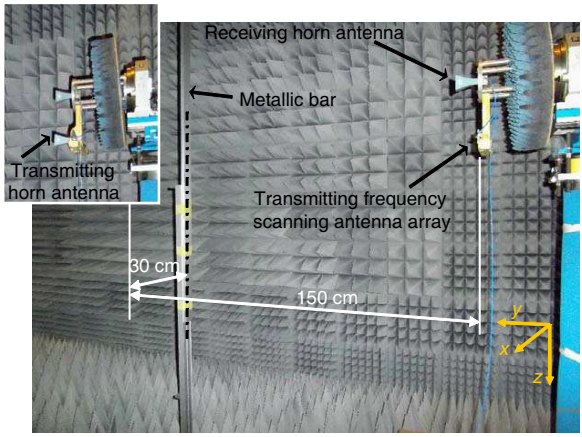

Figure 13. Scattered field measurement setup using the FSAA as transmitter and a horn antenna as receiver, when the metallic bar is placed at the position depicted in Figure 14. The upper left picture shows the measurement setup when two horn antennas are used.

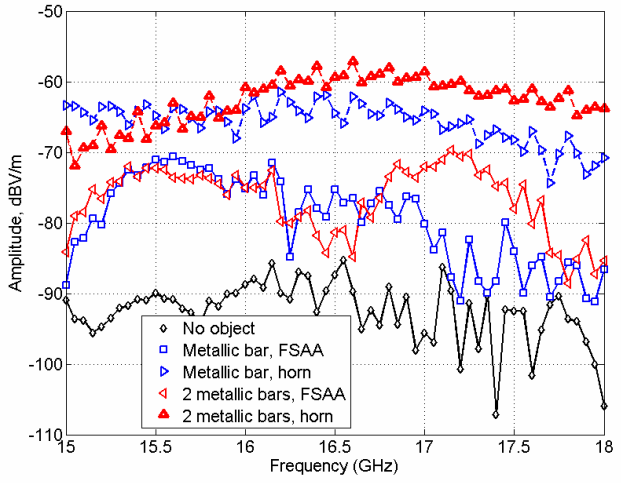

Figure 14. Measured electric field (E_x component, amplitude in dBV/m).

at the same distance from the Tx/Rx antennas. The scattered fields have been collected again from 15 to 18 GHz in 50 MHz steps. Figure 14 represents the measured scattered fields for this case and the previous one, including a situation in which no objects are present: the latter

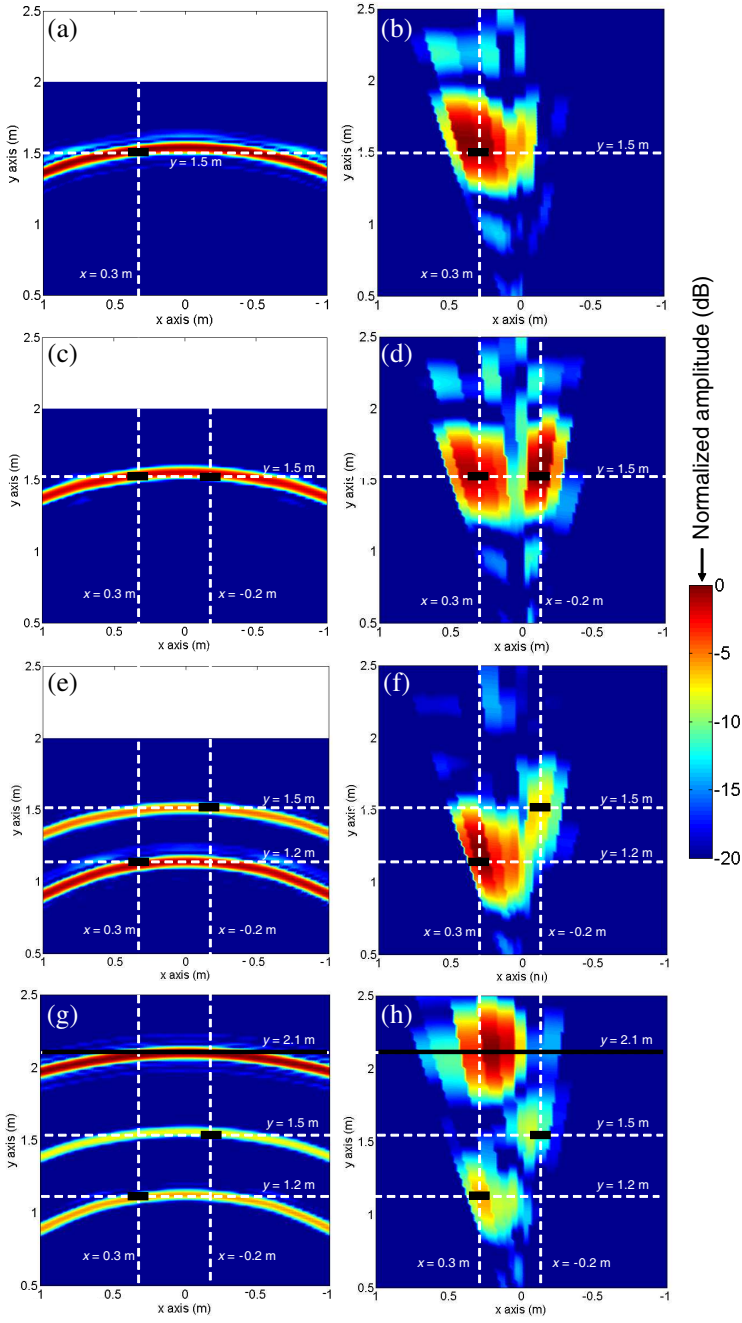
(a)
(b)
(c)
(d)
(e)
(f)
(g)
(h)
y = 1.5 m
y = 1.2 m
y = 2.1 m
x = 0.3 m
x = -0.2 m
y axis (m)
x axis (m)
Normalized amplitude (dB)
0
-5
-10
-15
-20

Figure 15. Retrieved SAR image (normalized amplitude, in dB). Black rectangles indicate the placement of the metallic bars and the plate. Coordinate system is referred to the FSAA position. (a), (c), (e), (g) Using a horn antenna as transmitter. (b), (d), (f), (h) Using the FSAA as transmitter, with $\Delta BW = 300\,\text{MHz}$ window. (a), (b) One metallic bar placed at $x = 0.3\,\text{m}$, $y = 1.5\,\text{m}$. (c), (d) Two metallic bars placed at the same distance in y-axis. (e), (f) Two metallic bars placed at different distance in y-axis. (g), (h) Two metallic bars and a plate placed at $y = 2.1\,\text{m}$.

is intended to give an idea of the measurement setup dynamic range.

Results are depicted in Figures 15(c), (d). The first case, Figure 15(c) corresponds to the use of the horn antenna as a transmitter. The range position of the bars is clearly identified ($\sim 1.5\,\text{m}$). When the FSAA is introduced, also the angular position is resolved. In order to remark the range-angular position trade-off of the FSAA imaging system, Figures 16(a)–(c) show the results for frequency windows of $\Delta BW = 200\,\text{MHz}$, $300\,\text{MHz}$, and $500\,\text{MHz}$. As expected, a narrow frequency window provides higher angular resolution, and a wide window improves range estimation. Combination of both images will improve the position estimation accuracy.

Two more configurations have been analyzed: the first one is depicted in Figures 15(e), (f). In this case, the two metallic bars are placed at different range and cross-range positions, so the reflectivity levels are different due to the field attenuation with the distance (as this parameter is not taken into account in Equation (1)). Again, when transmitting with the horn antenna, only range information is provided, identifying two objects at distances of $1.2\,\text{m}$ and $1.5\,\text{m}$ respectively (Figure 15(e)). By introducing the FSAA, the cross-range position is also estimated (Figure 15(f)).

The last case consists on a metallic plate of $2.5\,\text{m}$ along x axis and $1\,\text{m}$ along z axis (height) placed behind the two metallic bars, in the plane $y = 2.1\,\text{m}$ (see Figure 17). The goal is to analyze the influence of a strong scatterer in the imaging system. The use of the horn antenna as a transmitter allows identifying the range position of the 3 scatterers (Figure 15(g)). The metallic plate distance corresponds to the points having specular reflection with respect to the Tx/Rx. FSAA results also provide a rough guess of the metallic plate shape (a line parallel to the x axis). However, only the points close to the specular reflection exhibit high reflectivity values (Figure 15(h)). Also the shadow due to the metallic bar placed at $(x, y) = (-0.2, 1.5)\,\text{m}$ can be observed in the reconstructed SAR image.

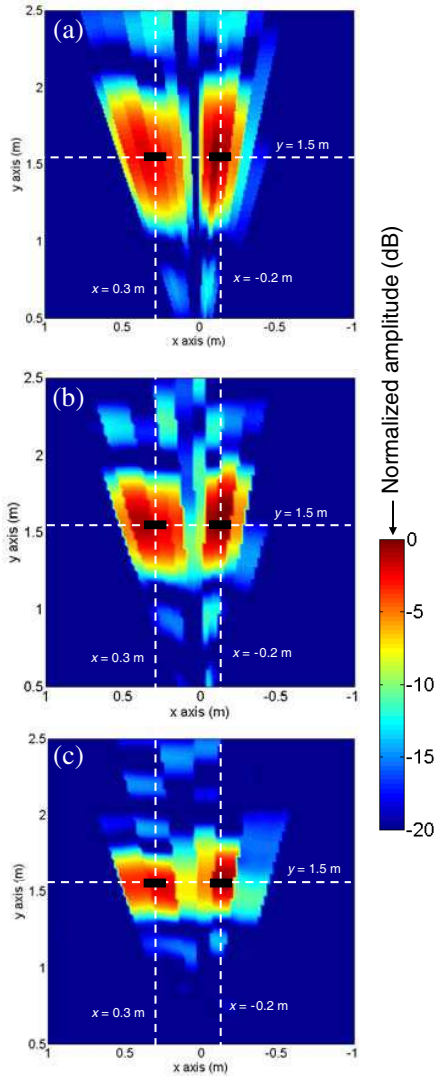

Figure 16. Retrieved SAR image (normalized amplitude, in dB). Black rectangles indicate the placement of the metallic bars. Coordinate system is referred to the FSAA position. (a) 200 MHz window. (b) 300 MHz window. (c) 500 MHz window.

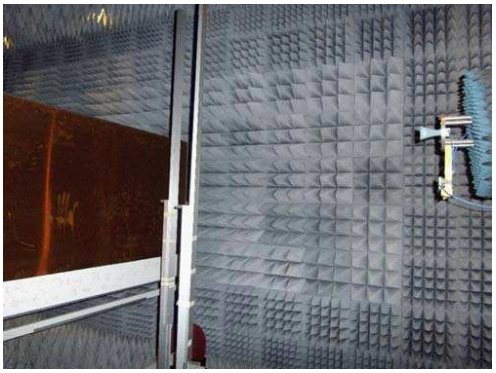

Figure 17. Two metallic bars placed at $(x, y) = (0.3, 1.2)$ and $(-0.2, 1.5)$ m, together with a metallic plate at $y = 2.1$ m.

5. CONCLUSIONS

A study of the FSAA imaging system features has been presented. The technique is conceived as a low-cost solution to obtain angular information of the target in range-based systems in which the antenna beam cannot be steered, either mechanically or using electronic variable phase shifting networks. A detailed analysis of the main parameters (number of antenna array elements, element phase shift, and frequency window bandwidth) influencing the range and cross-range resolution has been carried out, supported by simulation and measurement examples. Experimental results also confirm the system capacity to estimate the range and cross-range position of several metallic objects. Further work is devoted to improve FSAA features, aiming to extend system capabilities not only for objects detection, but also for shape reconstruction.

ACKNOWLEDGMENT

Manuscript received June 30, 2012. This work has been supported by the "Ministerio de Ciencia e Innovación" of Spain/FEDER under projects CONSOLIDER-INGENIO CSD2008-00068 (TERASENSE), TEC2011-24492/TEC (iSCAT), IPT-2011-0951-390000 (TECNIGRAF), and under PhD grant BES-2009-024060; by PCTI Asturias under projects EQUIP08-06, FC09-COF09-12, EQUIP10-31, and PC10-06 (FLEXANT).

REFERENCES

1. Sheen, D. M., D. L. McMakin, and T. E. Hall, "Three-dimensional millimeter-wave imaging for concealed weapon detection," *IEEE Transactions on Microwave Theory and Techniques*, Vol. 49, No. 9, 1581–1592, Sep. 2001.
2. Martinez-Lorenzo, J. A., C. M. Rappaport, and F. Quivira, "Physical Limitations on detecting tunnels using underground-focusing spotlight synthetic aperture radar," *IEEE Transactions on Geoscience and Remote Sensing*, Vol. 49, No. 1, 65–70, Jan. 2011.
3. Bond, E. J., X. Li, S. C. Hagness, and B. D. Van Veen, "Microwave imaging via space-time beamforming for early detection of breast cancer," *IEEE Transactions on Antennas and Propagation*, Vol. 51, No. 8, 1690–1705, Aug. 2003.
4. Colton, D. and A. Kirsch, "A simple method for solving inverse scattering problems in the resonance region," *Inverse Problems*, Vol. 12, No. 4, 383–393, Aug. 1996.
5. Álvarez López, Y., A. Domínguez-Casas, C. García-González, and F. Las-Heras, "Geometry reconstruction of metallic bodies using the sources reconstruction method," *IEEE Antennas and Wireless Propagation Letters*, Vol. 9, 1197–1200, 2010.
6. Pastorino, M., A. Massa, and S. Caorsi, "A microwave inverse scattering technique for image reconstruction based on a genetic algorithm," *IEEE Transactions on Instrumentation and Measurement*, Vol. 49, No. 3, 573–578, Jun. 2000.
7. Bozza, G., C. Estatico, M. Pastorino, and A. Randazzo, "An inexact newton method for microwave reconstruction of strong scatterers," *IEEE Antennas and Wireless Propagation Letters*, Vol. 5, No. 1, 61–64, Dec. 2006.
8. Lin, C.-Y. and Y.-W. Kiang, "Inverse scattering for conductors by the equivalent source method," *IEEE Transactions on Antennas and Propagation*, Vol. 44, No. 3, 310–316, Mar. 1996.
9. Caorsi, S., G. L. Gragnani, and M. Pastorino, "Two-dimensional microwave imaging by a numerical inverse scattering solution," *IEEE Transactions on Microwave Theory and Techniques*, Vol. 38, No. 8, 981–980, Aug. 1990.
10. Çayören, M., I. Akduman, A. Yapar, and L. Crocco, "A new algorithm for the shape reconstruction of perfectly conducting objects," *Inverse Problems*, Vol. 23, No. 3, 1087–1100, Jun. 2007.
11. Farmahini-Farahani, M., R. Faraji-Dana, and M. Shahabadi, "Fast and accurate cascaded particle swarm gradient optimization

method for solving 2-D inverse scattering problems," *Applied Computational Electromagnetics Society*, Vol. 24, No. 5, 2009.

12. Van den Berg, P. M. and R. E. Kleinman, "A contrast source inversion method," *Inverse Problems*, Vol. 13, No. 6, 1607–1620, Dec. 1997.
13. LaHaie, I. J., "Overview of an image-based technique for predicting far-field radar cross section from near-field measurements," *IEEE Antennas and Propagation Magazine*, Vol. 45, No. 6, 159–169, Dec. 2003.
14. Broquetas, A., J. Palau, L. Jofre, and A. Cardama, "Spherical wave near-field imaging and radar cross-section measurement," *IEEE Transactions on Antennas and Propagation*, Vol. 46, No. 5, 730–735, May 1998.
15. Lopez-Sanchez, J. M. and J. Fortuny-Guasch, "3-D radar imaging using range migration techniques," *IEEE Transactions on Antennas and Propagation*, Vol. 48, No. 5, 728–737, May 2000.
16. Llombart, N., R. J. Dengler, and K. B. Cooper, "Terahertz antenna system for a near-video-rate radar imager," *IEEE Antennas and Propagation Magazine*, Vol. 52, No. 5, 252–259, Oct. 2010.
17. Tran, H., F. Gumbmann, J. Weinzierl, and L.-P. Schmidt, "A fast scanning w-band system for advanced millimetre-wave short range imaging applications," *3rd European Radar Conference, EuRAD 2006*, 146–149, 2006.
18. Ranzani, L., N. Ehsan, and Z. Popoviać, "G-band frequency-scanned antenna arrays," *IEEE 2010 Antennas and Propagation Society International Symposium*, 1–4, Toronto, Canada, 2010.
19. Hilburn, J. and F. Prestwood, "K band frequency-scanned waveguide array," *IEEE Transactions on Antennas and Propagation*, Vol. 22, No. 2, 340–341, Mar. 1974.
20. Danielsen, M. and R. Jorgensen, "Frequency scanning microstrip antennas," *IEEE Transactions on Antennas and Propagation*, Vol. 27, No. 2, 146–150, 1979.
21. Ranzani, L., N. Ehsan, and Z. Popoviać, "G-band frequency-scanned antenna arrays," *IEEE 2010 Antennas and Propagation Society International Symposium*, 1–4, Toronto, Canada, Jul. 11–17, 2010.
22. Mayer, W., M. Wetzel, and W. Menzel, "A novel direct-imaging radar sensor with frequency scanned antenna," *IEEE MTT-S International Microwave Symposium Digest*, Vol. 3, 1941–1944, Philadelphia, U.S., Jun. 8–13, 2003.

23. Alvarez, Y., J. A. Martínez, F. Las-Heras, and C. M. Rappaport, "An inverse fast multipole method for geometry reconstruction using scattered field information," *IEEE Transactions on Antennas and Propagation*, Vol. 60, No. 7, 3351–3360, Jul. 2012.
24. Vazquez, C., S. Ver-Hoeye, M. Fernández, L. F. Herrán, and F. Las-Heras, "Frequency scanning probe for microwave imaging," *IEEE 2010 Antennas and Propagation Society International Symposium*, 1–4, Toronto, Canada, 2010.
25. Álvarez, Y., F. Las-Heras, and M. R. Pino, "Reconstruction of equivalent currents distribution over arbitrary three-dimensional surfaces based on integral equation algorithms," *IEEE Transactions on Antennas and Propagation*, Vol. 54, 3460–3468, Dec. 2007.
26. Álvarez, Y., F. Las-Heras, M. R. Pino, and T. K. Sarkar, "An improved super-resolution sources reconstruction method," *IEEE Transactions on Instrumentation and Measurement*, Vol. 58, No. 11, 3855–3866, Nov. 2009.
27. Quijano, J. L. A. and G. Vecchi, "Field and source equivalence in source reconstruction on 3D surfaces," *Progress In Electromagnetics Research*, Vol. 103, 67–100, 2010.